



Deposition of Columnar-Morphology Lanthanum Zirconate Thermal Barrier Coatings by Solution Precursor Plasma Spraying

Maryam Yaghtin¹ · Amirhossein Yaghtin^{1,2} · Pooria Najafisayar³ · Zhaolin Tang^{1,4} · Tom Troczynski¹

Submitted: 5 May 2021 / in revised form: 25 August 2021 / Accepted: 26 August 2021 / Published online: 5 October 2021
© ASM International 2021

Abstract Two types of precursor solutions, including lanthanum nitrate and lanthanum chloride, with zirconium acetate, were used to produce lanthanum zirconate coatings by solution precursor plasma spraying (SPPS). Thermal behavior of the precursor solutions, their rheological properties and atomization patterns were investigated by TGA–DSC, viscosity, surface tension and droplet size measurements, respectively. The chloride precursor led to the formation of impure lanthanum zirconate powder including LaOCl and ZrO₂, while the nitrate precursor combined with zirconium acetate produced pure lanthanum zirconate powder after pyrolysis. Increasing the salt concentration from 0.125 to 0.5 M led to the formation of solutions with ~ 2.7 times higher viscosity but ~ 7% lower surface tension. The ethanol based solutions had smaller surface tension compared to the water based (24.3 mN/m vs. 62.7 mN/m), while being more viscous (4.8 cp vs. 3.2 cp). The most significant factor affecting the droplet size in atomized solutions was their viscosity. The 0.5 M water-based solutions with about 28 μm median size droplets injected into the plasma plume produced columnar morphology coatings with ~ 23 vol.% porosity.

Keywords columnar structure · lanthanum zirconate · solution precursor plasma spraying

Introduction

Lanthanum zirconate, La₂Zr₂O₇ (LZ) is a promising top coat material for the next generation of thermal barrier coatings (TBCs) (Ref 1, 2). This ceramic material, with a pyrochlore structure, has shown superior thermo-physical properties compared to the other traditional TBC systems. Currently, 8YSZ (zirconia with 7–8 wt.% yttria addition) is the most common standard ceramic top coat material for TBC. It meets most of TBC requirements, i.e., high melting point (2680 °C) (Ref 3), a relatively low thermal conductivity (2.0–2.3 W.m⁻¹.K⁻¹ at ~ 1000 °C for a fully dense bulk; 0.9–1.2 W.m⁻¹.K⁻¹ for 10–15% porosity) (Ref 4, 5), a relatively high CTE (11 × 10⁻⁶ /K at ~ 1000 °C) (Ref 3) and good thermal and chemical stability (Ref 2, 6, 7). However, its use is limited to ~ 1200 °C because of the degradation mechanisms related to phase transformations and the resulting volume change, as well as high diffusivity of oxygen leading to bond coat oxidation and the relatively fast sintering of YSZ. The t' phase of YSZ decomposes into equilibrium tetragonal (t) and cubic (c) phases; upon cooling, the t phase transforms to the monoclinic (m) phase causing a ~ 4% volume expansion (Ref 1, 8). Additionally, YSZ coatings densify in-service through sintering which leads to an increase in their thermal conductivity and Young's modulus. These changes in the phase composition and microstructure of the coatings are accompanied by variations in the TBC properties, contributing to thermally-induced stresses, reduced coating's lifetime and eventually its failure (Ref 3, 9).

✉ Maryam Yaghtin
myaghtin@mail.ubc.ca

¹ Department of Materials Engineering, University of British Columbia, Vancouver, BC V6T 1Z4, Canada
² Department of Materials Science and Engineering, College of Chemical and Metallurgical Engineering, Shiraz Branch, Islamic Azad University, Shiraz, Iran
³ Department of Materials Science and Engineering, School of Engineering, Shiraz University, 7134851154 Shiraz, Iran
⁴ Northwest Mettech Corporation, Surrey, BC V4N 4C4, Canada

Lanthanum zirconate, on the other hand, has phase stability (no phase transition from room temperature to its melting point, i.e., 2295 °C), low thermal conductivity (1.55–2.15 W.m⁻¹.K⁻¹ at ~ 1000 °C for dense bulk and 0.68–0.87 W.m⁻¹.K⁻¹ at ~ 1000 °C for porous one), no “oxygen transparency” (i.e., relatively low diffusivity of oxygen) and sintering rate significantly lower than YSZ (Ref 1). Since LZ powder is not commercially available, several methods have been applied to fabricate LZ powders, such as solid-state reaction, co-precipitation, sol-gel, hydrothermal and molten salt methods (Ref 10–13). According to the ZrO₂-La₂O₃ phase diagram (Ref 1), for the molar ratio of ZrO₂ / La₂O₃ is 2:1, only a single LZ cubic phase is seen from room temperature to its melting point. J. Zhang et al. studied the in-situ phase stability of LZ from room temperature to 1400 °C by synchrotron x-ray diffraction (XRD) at Argonne National Laboratory (Ref 14).

Like other TBC top coats, LZ is commonly deposited by APS (i.e., using dry powders) or EB-PVD techniques. Liquid injection of feedstock has made suspension plasma spraying (SPS) and solution precursor plasma spraying (SPPS) two promising techniques to produce finely (nano or submicron sizes) structured coatings. Nanosized LZ particles were produced by Wang et al. through hydrothermal method with the precursors of the La(NO₃)₄ and Zr(NO₃)₄ solution to deposit LZ coatings by SPS (Ref 15). The deposited coating was a single phase (pyrochlore) LZ coating with ultrafine splats and 6–10 vol.% porosity. Weber et al. deposited LZ coatings by spray pyrolysis (Ref 16). In their studies, zirconyl oxynitrate hydrate (ZrO(NO₃)₂·xH₂O) and lanthanum nitrate hexahydrate (La(NO₃)₃·6H₂O) were dissolved in deionized water at a molar ratio of 1:1. The precursor solution was sprayed at the flow rate of 1 ml/min at 240 °C. The deposited coatings were calcined at 500–600 °C to decompose the nitrates into carbonates and finally into oxides. Vertical cracks developed in the coatings at the latest stage of the decomposition process. This is generally considered as a positive feature of TBC coating, providing strain tolerance and, thus, aiding in their thermal cycling resistance (Ref 17, 18).

Solution precursor plasma spraying (SPPS) can produce finely (nano- or submicron- sized) structured coatings from metallic salt solutions (Ref 17, 19). SPPS is a recent development in liquid feedstock spraying, in which the solution is injected into the plasma as the feedstock. The salt decomposes and oxidizes in-flight, forming oxide particles. SPPS coatings have the potential to exhibit high strain tolerance through introduction of vertical cracks, and have relatively low thermal conductivity due to the presence of submicron and nano-sized interconnected porosity with improved bond strength (Ref 20, 21). These properties combine the advantages of EB-PVD and APS processes

(Ref 21). Chemical precursors for SPPS (salts or organometallics of the respective ceramic powders, such as nitrates, acetates, chlorides, isopropoxides, and other combinations) undergo endothermic or exothermic chemical reactions, or a combination of both during pyrolysis. It is possible to have precursors that contain both oxidizing and reducing agents simultaneously. For instance, YSZ TBCs are typically deposited from acetate/ nitrate combinations (Ref 18, 19).

When precursor solutions are used as feedstock (SPPS), the liquid rapidly atomizes (fragmentation of solution stream by aerodynamic break-up) and vaporizes after injection into the plasma jet. The atomized droplet size depends on a balance between the solution properties that resist the fragmentation (i.e., surface tension and viscosity) and the plasma shear forces that break up the solution stream into fine droplets (Ref 22, 23). The following steps include precipitation or gelation, particle pyrolysis, melting, and finally impacting of the molten droplets with average sizes up to a few micrometers, onto the substrate (Ref 20, 21, 24–26). SPPS coating's microstructure and therefore its properties result from particle in-flight interaction with the plasma jet. The in-flight characteristics are in turn affected by the solution properties and the liquid injection method into the plasma stream. The microstructure and performance of SPPS coatings are affected by both “solution properties” such as surface tension, viscosity and density as well as “spraying parameters” e.g., plasma power, enthalpy and spray distance (Ref 23, 27). There is industrial demand to increase the SPPS coating deposition rate by feeding high concentrations of solutions. However, due to the saturation limit of the precursor solution, injection challenges caused by viscosity increase, and increased density of the coating microstructure, solution concentrations is limited (Ref 17). Chen et al. investigated the effect of solution concentration on splat formation and microstructure of SPPS-7YSZ coatings (Ref 28). They found that low concentration solutions experienced surface precipitation in droplets and produce soft and porous coatings. On the other hand, solutions with higher concentrations experienced volume precipitation within the droplets and thus dense coatings formation by build-up of dense splats.

Wang et al. worked on preparing dense LZ coatings by SPPS (Ref 29). They investigated the effect of urea addition to the precursor solutions on SPPS reactions through detailed thermal analysis. The results showed that the exothermic reactions inside the plasma generated less than 30 kW/g, and thus were far smaller than the input power of plasma torch used in their work (110 kW) so can be ignored. Duarte et al. studied the effect of precursor counter-cations (nitrate, chloride, and acetate) on the splat size of SPPS-LZ coatings (Ref 30). Thermal properties of

different solutions and splat size were investigated, but not the coating's microstructure. To our knowledge, these are the only studies published to-date regarding LZ coatings deposited by SPPS, and the coatings microstructural analysis is not reported yet. Besides, there is a lack of fundamental study on the relationship between the solution properties (chemistry, concentration, surface tension and viscosity), atomized droplet size distribution and SPPS-LZ coating's morphology. No literature data are available on producing SPPS-LZ coatings for TBC with strain-tolerant microstructure, i.e., columnar morphology, or vertically cracked with 15–25 vol.% porosity.

In the present study, two types of precursor solutions, lanthanum nitrate and lanthanum chloride with zirconium acetate were used to produce lanthanum zirconate coatings by solution precursor plasma spraying (SPPS). Thermal behavior of the precursor solutions, their rheological properties and atomization pattern were investigated by TGA-DSC, viscosity, surface tension and droplet size measurements, respectively. Based on the results of thermal analysis and coating phase compositions, the optimum precursors mixture was selected with the aim to produce single-phase LZ coatings. Coating microstructure was studied by SEM, phase composition by XRD and porosity by image analysis method. The main focus of this study was to achieve and characterize pure LZ coatings with desired columnar microstructure for strain-tolerant TBCs.

Materials and Methods

Solutions Preparation and Characterization

La₂O₃ precursors with two different counter-cations (nitrate and chloride) were utilized in this study. Lanthanum nitrate hexahydrate, denoted as LaNT, (La(NO₃)₃·6H₂O, Sigma-Aldrich Corp., USA), lanthanum chloride heptahydrate, denoted as LaCL, (LaCl₃·7H₂O, Sigma-Aldrich Corp., USA) and zirconium acetate, denoted as ZrAC, (Zr(CH₃CO₂)₄, 15–16% in dilute acetate acid, Sigma-Aldrich Corp., USA) were used as the reactants. The solvents were deionized water, absolute ethanol and their mixture at 50/50 vol.%.

To prepare the solution mixtures, stoichiometric amounts of lanthanum and zirconium precursors were dissolved in the solvent at room temperature. Two aqueous mixtures (0.5 mol/L) of lanthanum and zirconium precursors with different chemical compositions were studied to investigate their effects on lanthanum zirconate (La₂Zr₂O₇) synthesis by SPPS:

- Solution A (LaNT-ZrAC^H): LaNT precursor combined with ZrAC in 1:1 molar ratio,

- Solution B (LaCL-ZrAC^H): LaCL precursor combined with ZrAC in 1:1 molar ratio.

The mixtures were dried at 120 °C for 21 h and calcined in furnace at 1000 °C for 2 h, followed with thermal analysis and phase identification tests.

In the next step, LaNT-ZrAC precursor mixture was selected to study the effects of solution concentration and solvent on the solution as well as the SPPS coatings' microstructure. LaNT-ZrAC precursor mixture was prepared in two different concentrations (0.125 and 0.5 mol/L) in water. Then, 0.5 mol/L solution was prepared with three solvents: water (LaNT-ZrAC^H solution), ethanol (LaNT-ZrAC^{Et} solution) and 50/50 vol.% mixture of water with ethanol (LaNT-ZrAC^{H-Et} solution). Table 1 presents the chemical compositions of all the five different precursor solutions studied in this article. Surface tension and rheology of the precursors were studied to reveal the influence of precursor concentration and solvent type on the precursor properties which in turn affect the SPPS coatings' microstructures.

2 ml of each precursor solution was evaluated by a Simultaneous Thermal Analyzer (STA) 6000 (PerkinElmer, Waltham, MA, USA), in nitrogen flowing at 20 ml/min and heating each sample to 1000 °C at a rate of 10 °C/min. The test procedure remained the same for all the samples. The Thermal Gravimetric Analysis (TGA) and Differential Scanning Calorimetry (DSC) data were obtained simultaneously from the same sample. Phase analysis of the dried and calcined powder was conducted using an x-ray diffractometer (Rigaku, Multiflex XRD) with Cu K_α radiation. The XRD patterns were collected in a 2θ range from 3° to 90°, with 0.02° angular steps. The XRD operation voltage and current were maintained at 40 kV and 40 mA, respectively.

The rheological characteristics of the solutions were studied using MCR 502 rheometer (Anton Paar, Graz, Austria) with cup and bob geometry, at room temperature. All the solution samples were tested under the same sample preparation and test procedure conditions. A Force Tensiometer (KRÜSS-K100 GmbH, Hamburg, Germany) device was used to study the surface tension of precursor solutions. All the measurements were made using Du Nouy Ring (Radius: 9.545 mm & Wire Diameter: 0.37 mm) lamella tear-off method. The accuracy and repeatability of the measurements were determined by measuring the surface tension of HPLC grade Hexane solution in triplicates. For all the samples, the surface tension was measured thrice, and average value is reported with standard deviation.

Droplet size distribution measurements were conducted in the University of Toronto, Centre for Advanced Coating Technologies, using the setup shown schematically in

Table 1 Chemical compositions of the precursor solutions

Solution name	Precursor mixture composition	Solvent	Concentration (<i>M</i>)
LaCL-ZrAC ^H	LaCl ₃ ·7H ₂ O + Zr(CH ₃ CO ₂) ₄	Water	0.5
LaNT-ZrAC ^H	La(NO ₃) ₃ ·6H ₂ O + Zr(CH ₃ CO ₂) ₄	Water	0.5
LaNT-ZrAC ^H (0.125)	La(NO ₃) ₃ ·6H ₂ O + Zr(CH ₃ CO ₂) ₄	Water	0.125
LaNT-ZrAC ^{Et}	La(NO ₃) ₃ ·6H ₂ O + Zr(CH ₃ CO ₂) ₄	Ethanol	0.5
LaNT-ZrAC ^{H-Et}	La(NO ₃) ₃ ·6H ₂ O + Zr(CH ₃ CO ₂) ₄	50/50 vol.-%-water/ethanol mixture	0.5

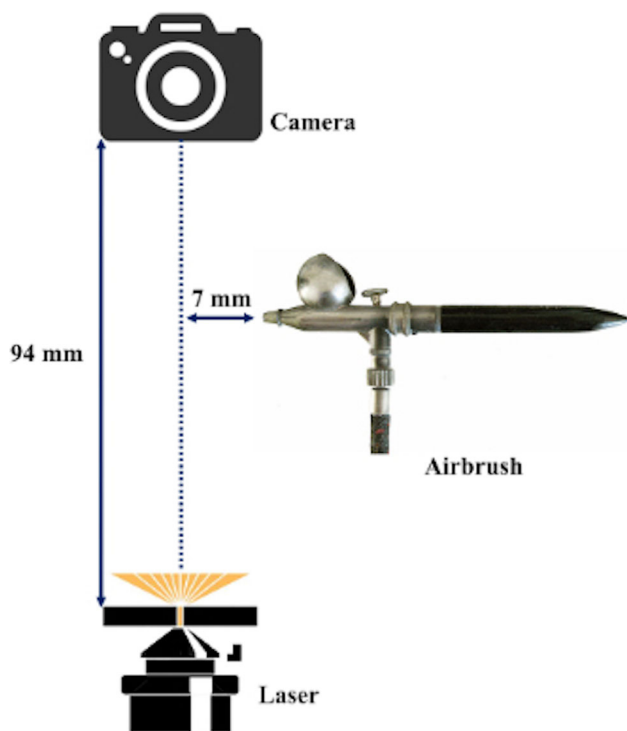
**Fig. 1** A schematic of the setup used for making comparison of droplet size distribution in different solutions

Fig. 1. The solution droplets were produced by an airbrush (Paasche H-Set Single Action Siphon Feed Airbrush Set) with 14 psi pressure. A home-made Dropsizer (DMCH001) was used to capture the images of droplets and by using ImageJ software (ImageJ– version 1.52a, National Institutes of Health, Maryland, USA), droplet size distributions were analyzed and compared. In fact, this is a high-speed camera using shadowgraphy technology to capture the very small and rapidly moving droplets. The laser is used for illumination, otherwise the droplets cannot be seen. For each sample, over 20 images were captured in four to five tests. In all, several thousands of droplets were recorded to assure accuracy of the analysis. As the depth of field of the camera is very small (0.23 mm) and as the mist of atomized droplets is a cone, there are always many blurred droplets on the images. Therefore, because of the non-symmetric

distributions, the median was calculated and reported rather than the average of the distributions to have a better estimate of the droplet size for each atomized solution. All the measurements were done under the same atomization condition for different samples.

Coatings Deposition and Characterization

Based on the solutions' characterization results, the optimized solutions of LaNT-ZrAC precursor mixtures (solution A) were used as the feedstock materials for solution precursor plasma spraying (SPPS). Inconel 718 sheet (2 mm thickness, cut into 0.6 mm × 0.6 mm square coupons) was used as the substrate material. The coupons were sand blasted and CoNiCrAlY bond coat (CO-210-24, Praxair Surface Technologies, Indianapolis, IN 46222, USA) was sprayed by Mettech Axial III (Northwest Mettech Corp., Surrey, Canada) APS system, Table 2. The ceramic top coats were deposited from the optimized solutions using the same Mettech Axial III high power plasma torch, but additionally equipped with a continuous stream solution injector system (LP-BT100-2J Peristaltic pump including a YZII15 pump head with three rollers). The SPPS parameters are also summarized in Table 2. The phase content and composition of the coatings were determined by XRD (Rigaku, Multiflex with Cu K_α radiation). The coated coupons were mounted in a low viscosity epoxy resin after vacuum infiltration, then, grinded and polished according to standard metallography procedures for TBCs. Morphology and microstructure of the coatings were investigated with Zeiss Sigma standard Field Emission Scanning Electron Microscope (FE-SEM). Porosity of the coatings was evaluated from SEM micrographs using image analyzer software (ImageJ– version 1.52a, National Institutes of Health, Maryland, USA). Due to the wide range of porosity length scale in the coatings (micron, submicron and nano pores), two different image magnifications were used for analyses: ×1000 (×1K) and ×10,000 (×10K). Features like inter-columnar spacing, big vertical cracks, and micro-sized pores can be captured in the low magnification images, while features like submicron and nano-sized pores can be found in the high magnification images.

Table 2 Atmospheric plasma spraying (APS) and solution precursor plasma spraying (SPPS) parameters utilized for bond coat and top coat deposition, respectively

Process	Powder feed rate (g/min)	Solution feed rate (mL/min)	Current (A)	Spray distance (mm)	Total plasma gas flow rate (SLM)	Plasma gas composition (Ar%/N ₂ %/H ₂ %)	Total torch power during spraying (kW)	Atomizing gas flow rate (SLM)	Nozzle internal diameter (mm)
APS	90	N/A	230	200	250	70/10/20	95	N/A	11
SPPS	N/A	30	230	60	180	40/40/20	105	25	9

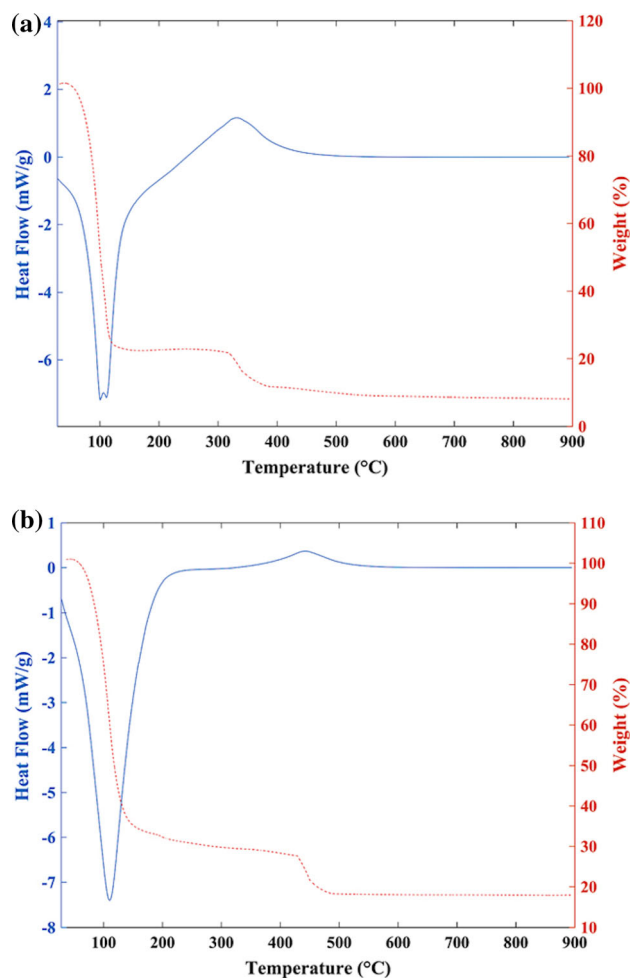
To evaluate the relative porosity values of the coatings, a total of 20 SEM micrographs were captured across each coating's cross section for both magnifications. All the images were threshold adjusted and converted into binary (black and white) images to calculate the porosity.

Results and discussion

Thermal behavior of precursor solutions

TGA-DSC analysis results attributed to the precursor solutions A (LaNT-ZrAC) and B (LaCL-ZrAC) are presented in Fig. 2. Two distinct successive mass loss regions are present for both samples; the first is attributed to solvent (water) evaporation starting from room temperature to around 100 °C, which is consistent with a broad endothermic peak in the same temperature range. In the case of precursor solution including lanthanum chloride (solution B), an exothermic peak is observed at around 450 °C, related to the formation of LaOCl compound as reported previously (Ref 31). The exothermic peak at 340 °C for solution A indicates pyrolysis of zirconium acetate and lanthanum nitrate (Ref 29, 31). Most of the weight loss occurs for both solutions before 500 °C, due to solvent evaporation and precursors decomposition. However, DSC curve for solution A indicates continuous exothermic reaction, while no comparable heat flow to sample B can be observed above 500 °C. Such heat flow pattern could be related to the formation of lanthanum zirconate compound.

X-ray diffraction patterns for the powders A and B calcined at 1000 °C for 2 h are shown in Fig. 3. The diffraction peaks attributed to LaOCl compound are present for powders B; pure lanthanum zirconate pyrochlore peaks are seen for powders A. It appears that formation of LaOCl hinders formation of lanthanum zirconate; this is in accordance with DSC results (Fig. 2) indicating insignificant heat flow to precursor solution B at high temperatures. Weber et al. compared TGA for lanthanum nitrate and lanthanum acetate precursors and claimed that the acetate precursor decomposes faster compared to the nitrate precursor (Ref 16). Accordingly, the precursor solution A

**Fig. 2** TGA-DSC analysis results attributed to the (a) precursor solution A and (b) precursor solution B

(LaNT-ZrAC) was selected for further investigations as reported below.

Properties of the Precursor Solutions

The effects of salt concentration and type of solvent on the resulting precursor solutions' viscosity are shown in Fig. 4. Water based solutions have lower viscosity (1.2 and 3.2 cp for 0.125 and 0.5 M concentrations, respectively) in

Fig. 3 X-ray diffraction patterns for the powders calcined at 1000 °C for 2 h: (a) precursor solution A and (b) precursor solution B

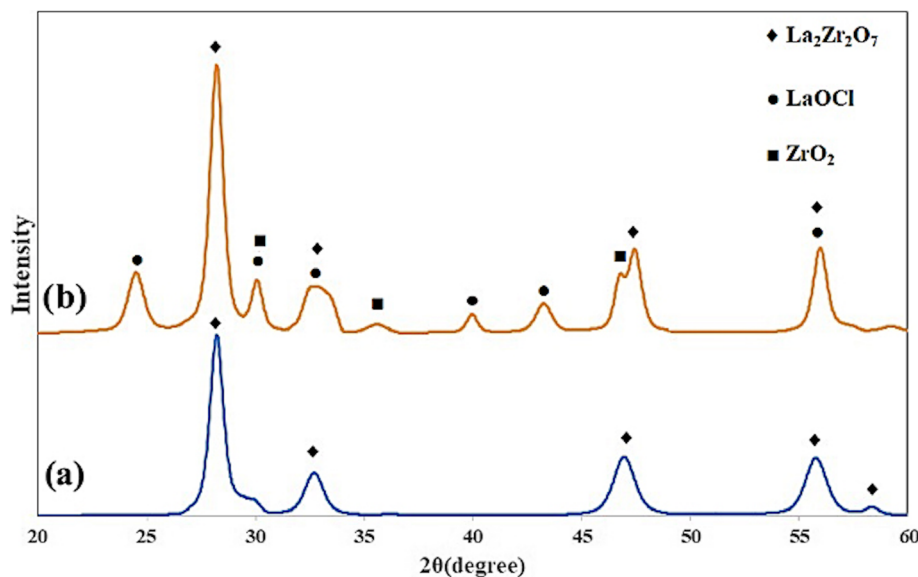
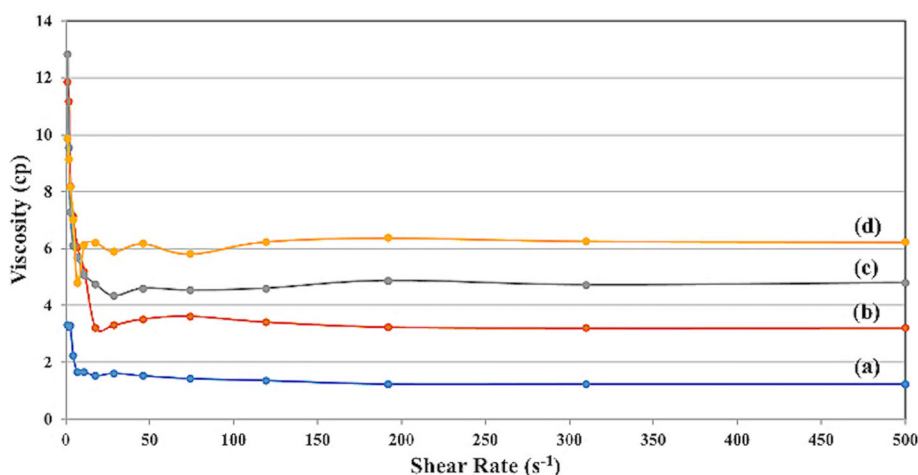


Fig. 4 Viscosity as a function of shear rate for: (a) water-based solution of 0.125 M LaNT-ZrAC^H, (b) water-based solution of 0.5 M LaNT-ZrAC^H, (c) ethanol-based solution of 0.5 M LaNT-ZrAC^{Et} and (d) 50/50 vol.-%-water/ethanol-based solution of 0.5 M LaNT-ZrAC^{H-Et}



comparison with those including ethanol (4.8 and 6.2 cp for ethanol based and mixed water/ethanol based 0.5 M solutions, respectively). The maximum viscosity was measured for the solution with 50/50 vol.-%-water/ethanol mixture, indicating that addition of ethanol to water has led to a substantial increase in viscosity. Such phenomenon has been attributed to enhanced water-ethanol molecules interactions (Ref 32). Increasing salt concentration in water based solutions from 0.125 to 0.5 M increased solution viscosity, as predicted by Jones-Dole expression, Eq. 1:

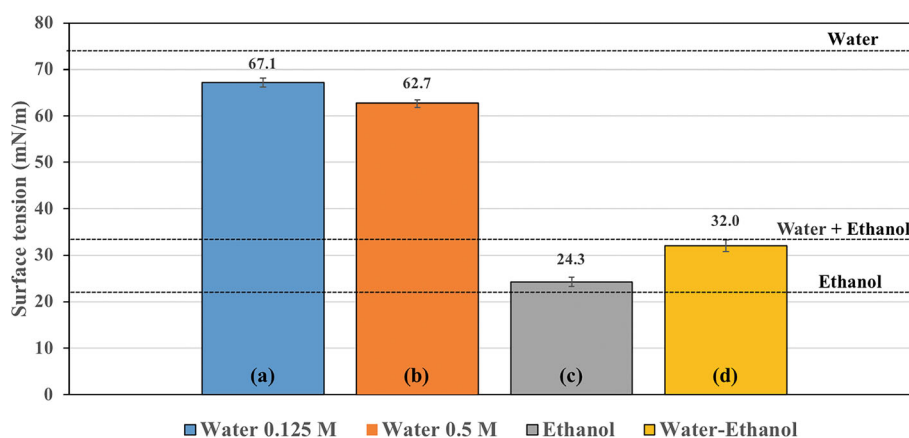
$$\frac{\eta}{\eta_0} = 1 + X\sqrt{C} + YC \quad (\text{Eq 1})$$

where η is the solution viscosity, η_0 is the solvent viscosity, X and Y are constants, and C is the salt concentration (Ref 33). It has been reported that formation of kosmotropic ions (structure-makers), because of salt dissociation in aqueous solutions, leads to increase in viscosity since such ions order the hydrogen bonding network in water. In contrast,

formation of structure-breaker ions (chaotropes) in water leads to decrease in viscosity by weakening the hydrogen network bonding (Ref 32, 33). In this regard, precursor salts such as lanthanum nitrate and zirconium acetate would be classified as those that produce kosmotropic ions since increasing their concentration in the solution resulted in larger viscosity. Such observations have been also reported previously in the case of preparation of other precursor solutions with different salt concentrations (Ref 28, 34, 35).

Figure 5 illustrates the variation in precursor solution surface tension as a function of its chemical composition. As seen, a decrease in surface tension from 62.7 ± 0.8 to 24.3 ± 0.2 mN/m is observed when the type of solvent is changed from water to ethanol at fixed salt concentration of 0.5 M. Surface tension values of 73.3, 22.8 and 33.2 mN/m were measured for pure water, pure ethanol, and 50/50

Fig. 5 Precursor solution surface tension for: (a) water-based solution of 0.125 M LaNT-ZrAC^H, (b) water-based solution of 0.5 M LaNT-ZrAC^H, (c) ethanol-based solution of 0.5 M LaNT-ZrAC^{E_t} and (d) 50/50 vol.-%-water/ethanol-based solution of 0.5 M LaNT-ZrAC^{H-E_t}. The dashed lines indicate surface tension of pure solvents



vol.-% mixture of water/ethanol, respectively, in agreement with the literature data (Ref 36, 37).

The surface tension values of the aqueous precursor mixtures (67.1 ± 0.9 and 62.7 ± 0.8 mN/m for LaNT-ZrAC^H with 0.125 and 0.5 M concentrations, respectively) were lower than that of the solvent's (73.3 mN/m). This is while the surface tension of 0.5 M LaNT^H, 72.4 mN/m, was close to that of water because nitrate (NO₃⁻) ion can be solvated and water has surface tension value similar to that of nitric acid (72.6 mN/m). The surface tension of 0.5 M ZrAC^H, on the other hand, was measured as 59.7 mN/m, which is lower than that of the water solvent. The acetate ion (CH₃COO⁻) is an amphiphilic compound (i.e., containing hydrophilic (COO⁻) and hydrophobic (CH₃) groups) and acts as a surfactant to decrease the surface tension. The acetate ion cannot solvate in aqueous media and converts to acetic acid which has a surface tension of 27.1 mN/m (Ref 36, 37); the surface tension of ZrAC^H is determined by both water and acetic acid. Consequently, it can be concluded that the effect of the acetate ion is more dominant than that of the nitrate ion in LaNT-ZrAC^H and LaNT-ZrAC^{H-E_t} solutions. The surface tension of alcoholic LaNT-ZrAC^{E_t} solution (24.3 ± 0.2 mN/m) is close to that of the ethanol solvent (22.8 mN/m). Such observations prove that nature of the precursor counter-cation controls the interactions with the solvent and therefore the surface tension of the solution at a constant concentration. The influence of mineral ions (such as NO₃⁻) on the surface tension of solutions is minimal, whereas organic ions (such as CH₃COO⁻) can considerably affect the solution's surface tension. Moreover, increasing salt concentration from 0.125 to 0.5 M results in only a slight decrease in the surface tension values from 67.1 ± 0.9 to 62.7 ± 0.8 mN/m. This also can be explained by the increased concentration of the acetate ion (CH₃COO⁻) around the water molecules, which acts as a surfactant and decreases the surface tension. Therefore, it seems that surface tension is not as effective as viscosity in determining the atomized droplet

size of solutions and the SPPS coatings' morphology as will be discussed in the following sections.

Droplet size distributions for different atomized precursor solutions are shown in Fig. 6. The median droplet size increases as the salt concentration increases in precursor solution (17.4 μm for 0.5 M concentration vs. 15.9 μm for 0.125 M concentration in water based solutions, LaNT-ZrAC^H). Increase of ethanol concentration from zero to 50 vol.-% does not make any significant change in the median size of the atomized droplets for 0.5 M salts, i.e., a slight increase from 17.4 μm for water based LaNT-ZrAC^H, to 17.5 μm for water/ethanol based LaNT-ZrAC^{H-E_t} was observed. Further increase in ethanol portion (from 50 to 100% vol.-%) of the solvent, led to a more considerable increase in the droplet median size to 19.5 μm for ethanol based LaNT-ZrAC^{E_t} solution. It has been reported that solutions with lower viscosity and surface tension would be atomized to smaller droplets due to having less resistance against liquid break up (Ref 22, 23). In this work we observed that the most prominent factor influencing the change in droplet size is the change in solution viscosity, i.e., by increasing the salt concentration or replacing water with ethanol, larger droplets will be formed in the atomized solutions.

Coatings Characteristics

XRD patterns for coatings deposited from different precursor solutions are presented in Fig. 7. All the solutions led to the formation of pyrochlore lanthanum zirconate coatings regardless of differences in their concentration and solvent type, in agreement with thermal analysis for LaNT-ZrAC. Cross-sectional morphologies of such coatings, all deposited at conditions listed in Table 2, are illustrated in Fig. 8. While the same number of spray passes (105) were applied for all the top coat depositions, results showed that the coatings deposited from dilute 0.125 M solutions are thinner (~ 22 to 35 μm) as compared to 0.5

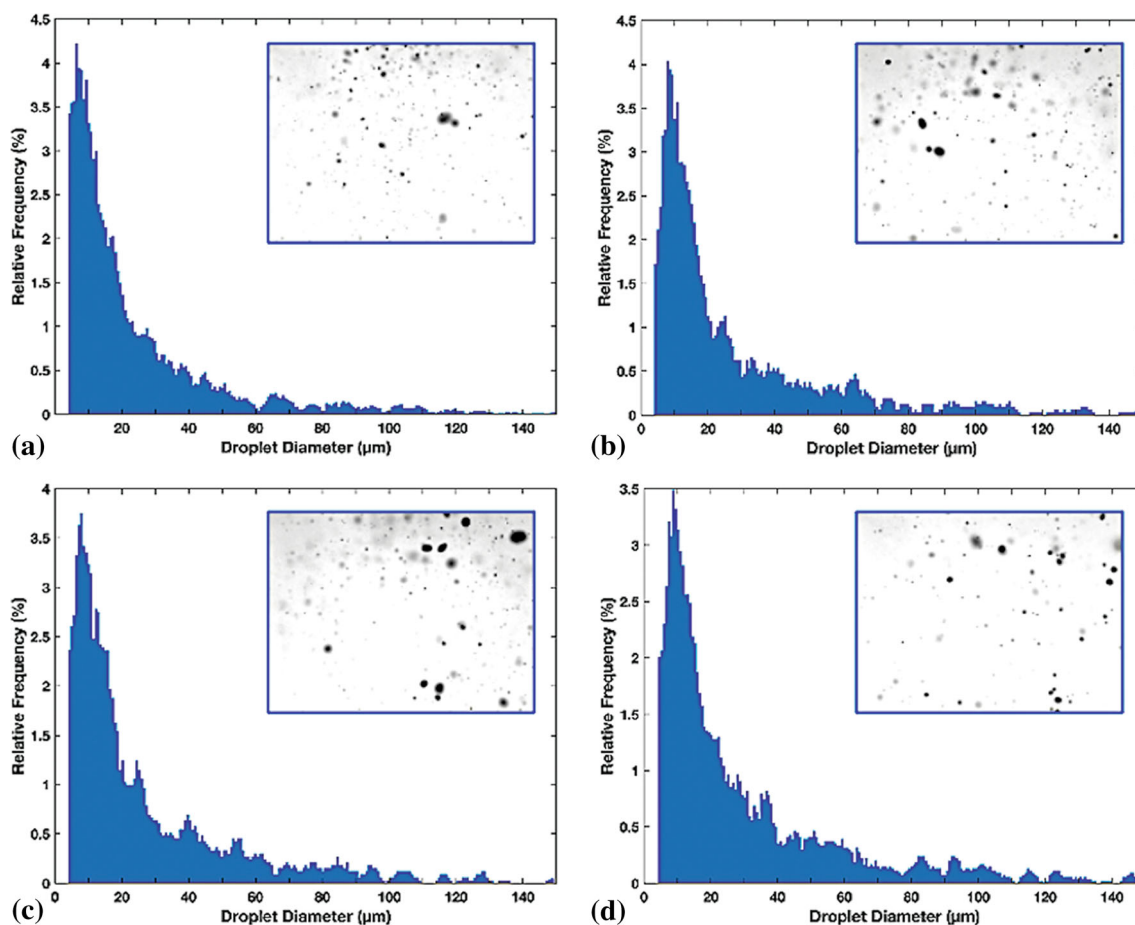


Fig. 6 Droplet size distributions for atomized precursor solutions (shown as subfigures above) of: (a) water based solution of 0.125 M LaNT-ZrAC^H, (b) water based solution of 0.5 M LaNT-ZrAC^H,

(c) ethanol based solution of 0.5 M LaNT-ZrAC^{Et} and (d) 50/50 vol.-%-water/ethanol based solution of 0.5 M LaNT-ZrAC^{H-Et}

M solutions (~ 120 to 140 μm). Such observations have been also reported in the case of other types of thermal barrier coatings that have been deposited by thermal spraying techniques (Ref 18, 38). The fact is that application of dilute precursor solutions results in formation of thinner coatings, at the fixed other deposition conditions like number of spray passes etc., because of shortage of starting material for the coating formation. Notably, the application of water-based precursor solutions resulted in the formation of coatings with columnar structure. It has been reported that as the droplets approach the substrate surface at more oblique angles, the probability of formation of coatings with columnar morphologies increases, based on shadow effect theory (Ref 18, 39). Stokes number *St*, Eq. 2, can be used to determine the influencing factors on the droplets' preferred approach angle to the substrate:

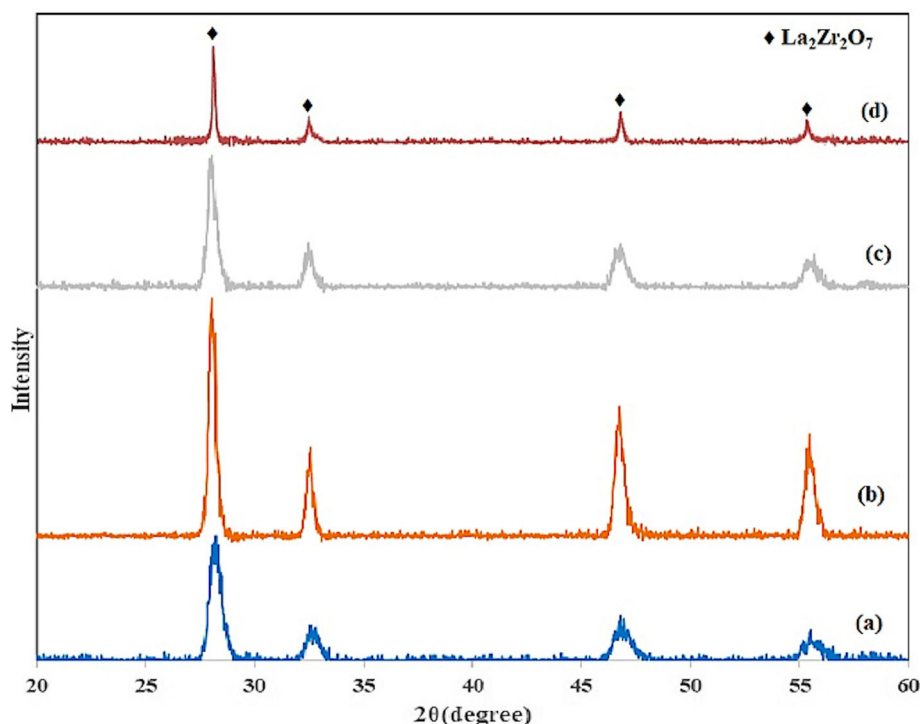
$$St = \frac{\rho d^2 v}{18 \mu l} \tag{Eq 2}$$

where ρ is the droplet density, d is the droplet diameter, v is the droplet velocity, μ is the plasma dynamic viscosity and

l is the boundary layer thickness. Relatively small Stokes number ($St < 1$) indicates increased probability of droplets approaching the substrate at more oblique angles (Ref 18, 39). Formation of columnar coatings from water based precursor solutions could be related to the small droplet sizes increasing the chance of having small Stokes numbers (Ref 40, 41). This is in accordance with the droplet size distribution measurements of atomized solutions as discussed above (17.4 and 15.9 μm for 0.5 and 0.125 M concentrations of water based solutions, respectively). In fact, small atomized droplets should produce small molten particles which impinge onto the substrate with more oblique angles than the larger ones. In some cases, incomplete pyrolysis of impinging droplets may produce so-called foamy microstructure including partially dried nitrates. Such phenomenon is not likely to occur in the present case since x-ray diffraction peaks of such compounds were not observed in the XRD patterns of the deposited coatings (Fig. 7).

Porosity of the coatings deposited from different precursor solutions is presented in Fig. 9. As seen, more

Fig. 7 XRD patterns for the coatings deposited from different precursor solutions: (a) water based solution of 0.125 M LaNT-ZrAC^H, (b) water based solution of 0.5 M LaNT-ZrAC^H, (c) ethanol based solution of 0.5 M LaNT-ZrAC^{Et} and (d) 50/50 vol.-%-water/ethanol based solution of 0.5 M LaNT-ZrAC^{H-Et}



porous (~ 23 vol.%) coatings were deposited from the water based precursor solutions. This could be related to partial solidification of the smaller droplets before their impact on the substrate, which in turn enhances void formation as the new semi-molten particles join previously deposited ones on the growing coating. Such observations have been also reported previously in the case of various types of SPPS and SPS coating processes (Ref 18, 23). Increasing the concentration from 0.125 to 0.5 M had no effect on coating porosity. The 0.5 M concentration for LaNT-ZrAC solution can still be considered as a relatively low concentration with respect to the salt's saturation limit. Increasing the concentration above 0.5 M leads to a decrease in the coating's porosity which is not desired in the case of TBCs. The ethanol-based coating was the most dense one (with 8.25 ± 0.37 vol.% porosity), while the water/ethanol-based coating had 15.8 ± 0.33 vol.% porosity value which is still acceptable for a typical TBC (Ref 42, 43).

Conclusions

Applicability of precursor solutions including lanthanum nitrate and lanthanum chloride with zirconium acetate to deposit lanthanum zirconate coatings by solution precursor

plasma spraying (SPPS) was assessed. Thermal analysis (TGA-DSC) and phase analysis (XRD) results showed that unlike the nitrate precursor mixtures, the chloride precursor solutions cannot provide pure lanthanum zirconate pyrochlore structure. Therefore, four different precursor solutions including lanthanum nitrate and zirconium acetate with different salt concentrations and water, ethanol and water/ethanol solvents were used for SPPS coatings deposition. Viscosity and surface tension measurements revealed that increasing the salt concentration results in higher viscosity and smaller surface tension values. Replacing water with ethanol solvent resulted in more viscous solutions with smaller surface tensions. Application of dilute water based solutions in SPPS led to the formation of porous (~ 23 vol.%) coatings with columnar morphology, which can be considered as a desirable, strain-tolerant microstructure for TBCs. In the selected solution concentration values, the 0.5 M concentration can be considered as the best one for our system, based on the achieved coating's thickness of about 120 to 140 μm and columnar morphology. This unique microstructure is related to the relatively low viscosity of such solutions (~ 1 to 3 cp) that results in the formation of relatively small droplets in the plasma plume, which then approach the substrate at more oblique angles preferable in the formation of the columnar microstructures.

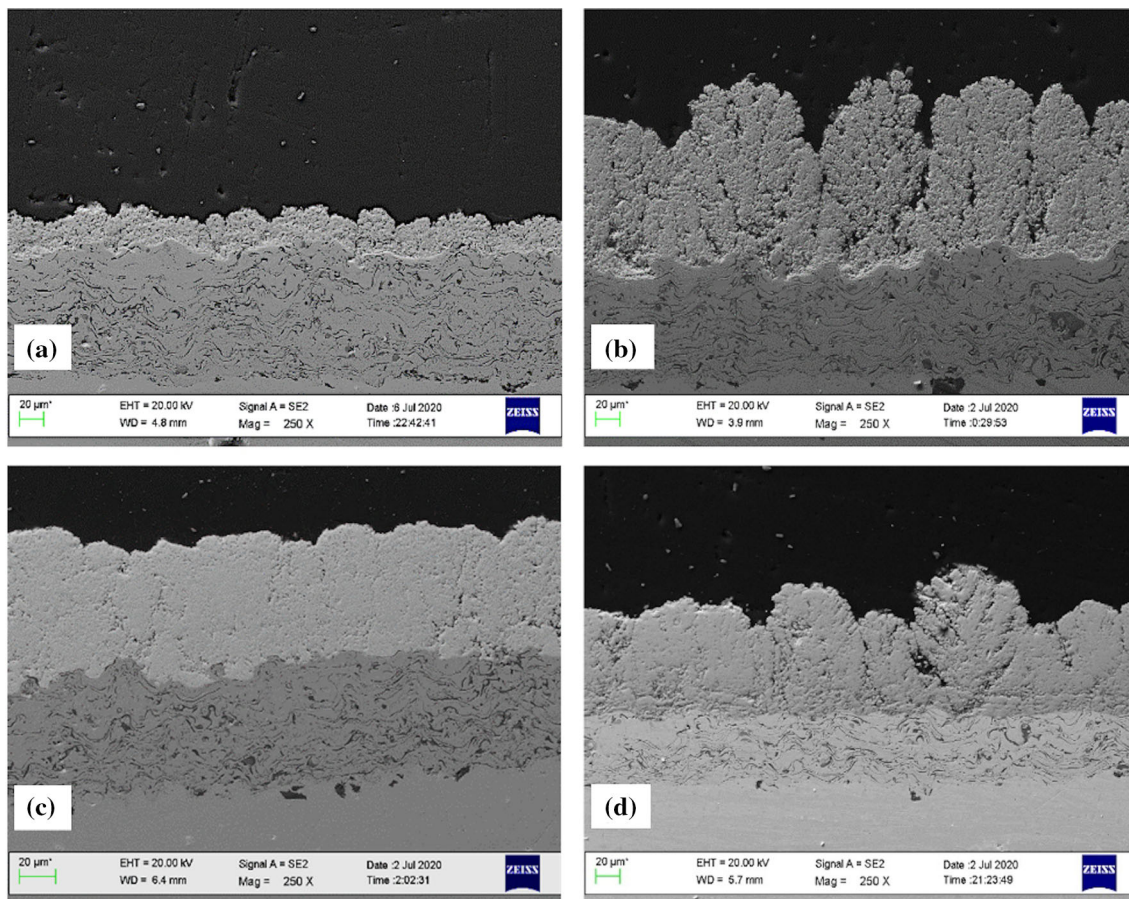
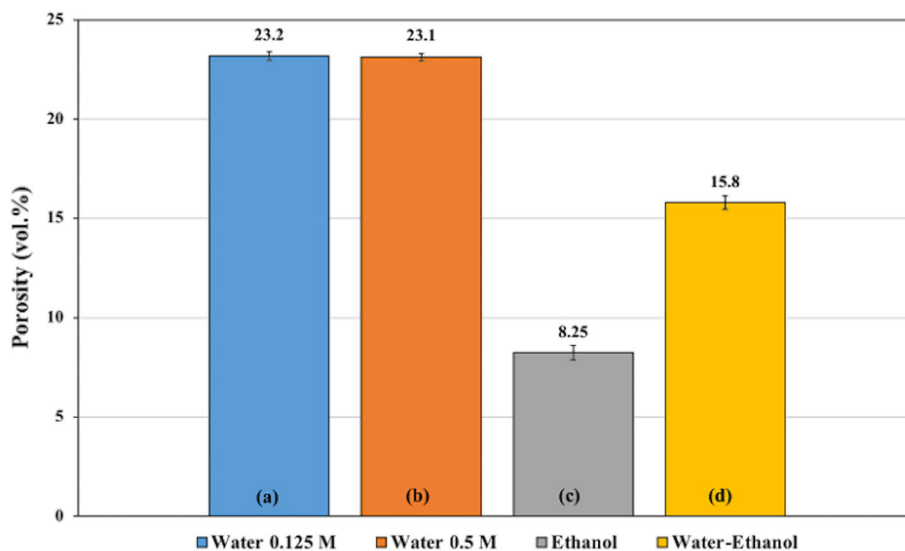


Fig. 8 Cross-sectional morphologies of the coatings deposited from different precursor solutions: (a) water-based solution of 0.125 M LaNT-ZrAC^H, (b) water-based solution of 0.5 M LaNT-ZrAC^H,

(c) ethanol-based solution of 0.5 M LaNT-ZrAC^{Et} and (d) 50/50 vol.-%-water/ethanol-based solution of 0.5 M LaNT-ZrAC^{H-Et}

Fig. 9 Estimated porosity for SPPS coatings obtained from different solutions: (a) water based solution of 0.125 M LaNT-ZrAC^H, (b) water based solution of 0.5 M LaNT-ZrAC^H, (c) ethanol based solution of 0.5 M LaNT-ZrAC^{Et} and (d) 50/50 vol.-%-water/ethanol based solution of 0.5 M LaNT-ZrAC^{H-Et}



Acknowledgments The authors would like to acknowledge the financial support of the Natural Science and Engineering Research Council Canada, within “Green Surface Engineering for Advanced Manufacturing” (Green-SEAM) Strategic Network, for this work. We

also express gratitude to Northwest Mettech Corporation for the collaboration in coatings deposition as well as the University of Toronto, Centre for advanced Coating Technologies, for droplet particle size distribution measurements.

References

- J. Zhang, X. Guo, Y. Jung, L. Li and J. Knapp, Lanthanum Zirconate Based Thermal Barrier Coatings: A Review, *Surf. Coatings Technol.*, 2017, **323**, p 18–29. <https://doi.org/10.1016/j.surfcoat.2016.10.019>
- V. Kumar and B. Kandasubramanian, Processing and Design Methodologies for Advanced and Novel Thermal Barrier Coatings for Engineering Applications, *Particuology*, 2016, **27**, p 1–28. <https://doi.org/10.1016/j.partic.2016.01.007>
- R. Vassen, X. Cao, F. Tietz, D. Basu and D. Stover, Zirconates as New Materials for Thermal Barrier Coatings, *J. Am. Ceram. Soc.*, 2000, **83**(8), p 2023–2028.
- D. Hasselman, L. Johnson, L.D. Bentsen, R. Syed, H.L. Lee and M.V. Swain, Thermal Diffusivity and Conductivity of Dense Polycrystal-Line ZrO₂ Ceramics: A Survey, *Am. Ceram. Soc. Bull.*, 1987, **66**(5), p 799–806.
- K.W. Schlichting, N.P. Padture and P.G. Klemens, Thermal Conductivity of Dense and Porous Yttria-Stabilized Zirconia, *J. Mater. Sci.*, 2001, **36**(12), p 3003–3010.
- X.Q. Cao, R. Vassen, W. Jungen, S. Schwartz, F. Tietz and D. Stover, Thermal Stability of Lanthanum Zirconate Plasma-Sprayed Coating, *J. Am. Ceram. Soc.*, 2001, **84**(9), p 2086–2090.
- D.F. Zambrano, A. Barrios, L.E. Tobón and C. Serna, Thermal Properties and Phase Stability of Yttria-Stabilized Zirconia (YSZ) Coating Deposited by Air Plasma Spray onto a Ni-base Superalloy, *Ceram. Int.*, 2018, **44**(4), p 3625–3635. <https://doi.org/10.1016/j.ceramint.2017.11.109>
- C. Jiang, E.H. Jordan, A.B. Harris, M. Gell and J. Roth, Double-Layer Gadolinium Zirconate/Yttria-Stabilized Zirconia Thermal Barrier Coatings Deposited by the Solution Precursor Plasma Spray Process, *J. Therm. Spray Technol.*, 2015, **24**(6), p 895–906. <https://doi.org/10.1007/s11666-015-0283-6>
- Z. Lu, M.S. Kim and S.W. Myoung, Thermal Stability and Mechanical Properties of Thick Thermal Barrier Coatings with Vertical Type Cracks, *Trans. Nonferrous Met. Soc. China*, 2014, **24**(1), p 29–35.
- M.A. Subramanian, G. Aravamudan and G.V. Subba Rao, Oxide Pyrochlore—A Review, *Prog. Solid State Chem.*, 1983, **15**(2), p 55–143.
- K.K. Rao, T. Banu, M. Vithal, G.Y.S.K. Swamy and K.R. Kumar, Preparation and Characterization of Bulk and Nano Particles of La₂Zr₂O₇ by Sol–Gel Method, *Mater. Lett.*, 2002, **54**(2–3), p 205–210.
- J. Nair, P. Nair, E.B.M. Doesburg and J.G. Van Ommen, Preparation and Characterization of Lanthanum Zirconate, *J. Mater. Sci.*, 1998, **33**(18), p 4517–4523. <https://doi.org/10.1023/A:1004496100596>
- X. Wang, Y. Zhu and W. Zhang, Preparation of Lanthanum Zirconate Nano-Powders by Molten Salts Method, *J. Non. Cryst. Solids*, 2010, **356**(20–22), p 1049–1051. <https://doi.org/10.1016/j.jnoncryst.2010.01.016>
- J. Zhang, X. Guo, Y. Jung, L. Li and J. Knapp, Microstructural Non-Uniformity and Mechanical Property of air Plasma-Sprayed Dense Lanthanum Zirconate Thermal Barrier Coating, *Mater. Today Proc.*, 2014, **1**(1), p 11–16. <https://doi.org/10.1016/j.matpr.2014.09.003>
- C. Wang, Y. Wang, L. Wang and G. Hao, Nanocomposite Lanthanum Zirconate Thermal Barrier Coating Deposited by Suspension Plasma Spray Process, *J. Therm. Spray Technol.*, 2014, **23**(7), p 1030–1036. <https://doi.org/10.1007/s11666-014-0068-3>
- S.B. Weber, H.L. Lein, T. Grande and M.A. Einarsrud, Deposition Mechanisms of Thick Lanthanum Zirconate Coatings by Spray Pyrolysis, *J. Am. Ceram. Soc.*, 2011, **94**(12), p 4256–4262. <https://doi.org/10.1111/j.1551-2916.2011.04807.x>
- E.H. Jordan, C. Jiang and M. Gell, The Solution Precursor Plasma Spray (SPPS) Process: A Review With Energy Considerations, *J. Therm. Spray Technol.*, 2015, **24**(7), p 1153–1165. <https://doi.org/10.1007/s11666-015-0272-9>
- A. Ganvir, R. Calinas, N. Markocsan, N. Curry and S. Joshi, Experimental Visualization of Microstructure Evolution During Suspension Plasma Spraying of Thermal Barrier Coatings, *J. Eur. Ceram. Soc.*, 2019, **39**(2–3), p 470–481. <https://doi.org/10.1016/j.jeurceramsoc.2018.09.023>
- N.P. Padture, K.W. Schlichting, T. Bhatia and A. Ozturk, Towards Durable Thermal Barrier Coatings With Novel Microstructures Deposited by Solution Precursor Plasma Spray, *Acta Mater.*, 2001, **49**, p 2251–2257. [https://doi.org/10.1016/S1359-6454\(01\)00130-6](https://doi.org/10.1016/S1359-6454(01)00130-6)
- E.H. Jordan, L. Xie, M. Gell and N.P. Padture, Superior Thermal Barrier Coatings Using Solution Precursor Plasma Spray, *J. Therm. Spray Technol.*, 2004, **13**(1), p 57–65. <https://doi.org/10.1361/10599630418121>
- P. L. Fauchais, J. V. R. Heberlein, and M. I. Boulos, *Thermal Spray Fundamentals: From Powder to Part*. New York, 2014.
- S. Basu and B.M. Cetegen, Modeling of Thermo-Physical Processes in Liquid Ceramic Precursor Droplets Injected into a Plasma Jet, *Int. J. Heat Mass Transf.*, 2007, **50**(17–18), p 3278–3290. <https://doi.org/10.1016/j.ijheatmasstransfer.2007.01.036>
- A. Ozturk and B.M. Cetegen, Modeling of Plasma Assisted Formation of Precipitates in Zirconium Containing Liquid Precursor Droplets, *Mater. Sci. Eng. A*, 2004, **384**(1–2), p 331–351. <https://doi.org/10.1016/j.msea.2004.06.042>
- C.K. Muoto, E.H. Jordan, M. Gell and M. Aindow, Identification of Desirable Precursor Properties for Solution Precursor Plasma Spray, *J. Therm. Spray Technol.*, 2011, **20**(4), p 802–816. <https://doi.org/10.1007/s11666-011-9636-y>
- P. Fauchais, G. Montavon, R.S. Lima and B.R. Marple, Engineering a New Class of Thermal Spray Nano-Based Microstructures from Agglomerated Nanostructured Particles, Suspensions and Solutions: An Invited Review, *J. Phys. D: Appl. Phys.*, 2011, **10**, p 111. <https://doi.org/10.1088/0022-3727/44/9/093001>
- S. Basu, E.H. Jordan and B.M. Cetegen, Fluid Mechanics and Heat Transfer of Liquid Precursor Droplets Injected into High-Temperature Plasmas, *J. Therm. Spray Technol.*, 2008, **17**(1), p 60–72. <https://doi.org/10.1007/s11666-007-9140-6>
- A. Ozturk and B.M. Cetegen, Modeling of Axially and Transversely Injected Precursor Droplets into a Plasma Environment, *Int. J. Heat Mass Transf.*, 2005, **48**(21–22), p 4367–4383. <https://doi.org/10.1016/j.ijheatmasstransfer.2005.05.015>
- D. Chen, E.H. Jordan and M. Gell, Effect of Solution Concentration on Splat Formation and Coating Microstructure Using the Solution Precursor Plasma Spray Process, *Surf. Coatings Technol.*, 2008, **202**(10), p 2132–2138. <https://doi.org/10.1016/j.surfcoat.2007.08.077>
- W.Z. Wang, T. Coyle and D. Zhao, Preparation of Lanthanum Zirconate Coatings by the Solution Precursor Plasma Spray, *J. Therm. Spray Technol.*, 2014, **23**(5), p 827–832. <https://doi.org/10.1007/s11666-014-0084-3>
- W. Duarte, S. Rossignol and M. Vardelle, La₂Zr₂O₇ (LZ) Coatings by Liquid Feedstock Plasma Spraying: The Role of Precursors, *J. Therm. Spray Technol.*, 2014, **23**(8), p 1425–1435. <https://doi.org/10.1007/s11666-014-0131-0>
- Y. Chen, Q. Qian, X. Liu, L. Xiao and Q. Chen, LaOCl Nano-fibers Derived from Electrospun PVA/Lanthanum Chloride Composite Fibers, *Mater. Lett.*, 2010, **64**(1), p 6–8. <https://doi.org/10.1016/j.matlet.2009.09.042>

32. A.H. Pelofsky, Surface Tension-Viscosity Relation for Liquids, *J. Chem. Eng. Data*, 1966, **11**(3), p 394–397. <https://doi.org/10.1021/je60030a031>
33. G. Jones and M. Dole, The Viscosity of Aqueous Solutions of Strong Electrolytes with Special Reference to Barium Chloride, *J. Phys. Chem.*, 1929, **51**, p 2950–2964.
34. H. Donald and B. Jenkins, Viscosity B-Coefficients of Ions in Solution, *Chem. Rev.*, 1995, **95**(8), p 2695–2724.
35. Y. Marcus, Effect of Ions on the Structure of Water, *Chem. Rev.*, 2009, **109**(3), p 1346–1370. <https://doi.org/10.1351/PAC-CON-09-07-02>
36. R.C. Weast, *CRC Handbook of Chemistry and Physics*, 62nd ed. CRC Press, Boca Raton, 1981.
37. D.R. Lide, *CRC Handbook of Chemistry and Physics*, 79th ed. CRC Press, Boca Raton, 1998.
38. R.T. Candidato, P. Sokołowski, L. Pawłowski and G. Lecomte-Nana, Development of Hydroxyapatite Coatings by Solution Precursor Plasma Spray Process and Their Microstructural Characterization, *Surf. Coat. Technol.*, 2017, **318**(3), p 39–49. <https://doi.org/10.1016/j.surfcoat.2016.10.072>
39. K. Vanevery, M.J.M. Krane, R.W. Trice, H. Wang and W. Porter, Column Formation in Suspension Plasma-Sprayed Coatings and Resultant Thermal Properties, *J. Therm. Spray Technol.*, 2011, **20**(4), p 817–828. <https://doi.org/10.1007/s11666-011-9632-2>
40. P. Fauchais, M. Vardelle, A. Vardelle and S. Goutier, What Do We Know, What are the Current Limitations of Suspension Plasma Spraying?, *J. Therm. Spray Technol.*, 2015, **24**(7), p 1120–1129. <https://doi.org/10.1007/s11666-015-0286-3>
41. F. Tarasi, E. Alebrahim, A. Dolatabadi and C. Moreau, Comparative Study of YSZ Suspensions and Coatings, *Coatings*, 2019 <https://doi.org/10.3390/COATINGS9030188>
42. M. Yaghtin, A. Yaghtin, P. Najafisayar, Z. Tang and T. Troczynski, Aging Behavior of Water-Based YSZ Suspensions for Plasma Spraying of Thermal Barrier Coatings. *J. Therm. Spray Technol.*, 2021.
43. A. Ganvir, S. Joshi, N. Markocsan and R. Vassen, Tailoring Columnar Microstructure of Axial Suspension Plasma Sprayed TBCs for Superior Thermal Shock Performance, *Mater. Des.*, 2018, **144**, p 192–208. <https://doi.org/10.1016/J.MATDES.2018.02.011>

Publisher's Note Springer Nature remains neutral with regard to jurisdictional claims in published maps and institutional affiliations.